

THE BEHAVIOR OF TRANSVERSE WAVES IN NONUNIFORM SOLAR FLUX TUBES. I. COMPARISON OF IDEAL AND RESISTIVE RESULTS

ROBERTO SOLER¹, MARCEL GOOSSENS², JAUME TERRADAS¹, AND RAMÓN OLIVER¹

¹Departament de Física, Universitat de les Illes Balears, E-07122, Palma de Mallorca, Spain and

²Centre for Mathematical Plasma Astrophysics, Department of Mathematics, KU Leuven, Celestijnenlaan 200B, 3001 Leuven, Belgium

Draft version April 27, 2022

ABSTRACT

Magnetohydrodynamic (MHD) waves are ubiquitously observed in the solar atmosphere. Kink waves are a type of transverse MHD waves in magnetic flux tubes that are damped due to resonant absorption. The theoretical study of kink MHD waves in solar flux tubes is usually based on the simplification that the transverse variation of density is confined to a nonuniform layer much thinner than the radius of the tube, i.e., the so-called thin boundary approximation. Here, we develop a general analytic method to compute the dispersion relation and the eigenfunctions of ideal MHD waves in pressureless flux tubes with transversely nonuniform layers of arbitrary thickness. Results for kink waves are produced and are compared with fully numerical resistive MHD eigenvalue computations in the limit of small resistivity. We find that the frequency and resonant damping rate are the same in both ideal and resistive cases. The actual results for thick nonuniform layers deviate from the behavior predicted in the thin boundary approximation and strongly depend on the shape of the nonuniform layer. The eigenfunctions in ideal MHD are very different from those in resistive MHD. The ideal eigenfunctions display a global character regardless of the thickness of the nonuniform layer, while the resistive eigenfunctions are localized around the resonance and are indistinguishable from those of ordinary resistive Alfvén modes. Consequently, the spatial distribution of wave energy in the ideal and resistive cases is dramatically different. This poses a fundamental theoretical problem with clear observational consequences.

Subject headings: Sun: oscillations — Sun: atmosphere — Sun: magnetic fields — waves — Magnetohydrodynamics (MHD)

1. INTRODUCTION

Transverse magnetohydrodynamic (MHD) waves are routinely observed in the solar atmosphere after the first detection of standing waves with TRACE (e.g., Nakariakov et al. 1999; Aschwanden et al. 1999) and of propagating waves with Hinode/SOT and CoMP (e.g., De Pontieu et al. 2007; Tomczyk et al. 2007). Kink waves are a specific type of almost incompressible transverse MHD waves in magnetic flux tubes (see, e.g., Edwin & Roberts 1983; Goossens et al. 2009, 2012a), which are damped by resonant absorption due to naturally occurring plasma inhomogeneity in the direction transverse to the magnetic field (e.g., Goossens et al. 1992, 2002; Ruderman & Roberts 2002; Pascoe et al. 2010; Terradas et al. 2010b; Soler et al. 2011b).

The theoretical study of kink MHD waves in solar flux tubes using normal modes usually relies on two simplifications: (1) the thin tube (TT) approximation, that assumes that the wavelength is much longer than the radius of the flux tube, and (2) the thin boundary (TB) approximation, that confines the transverse variation of density to a layer much thinner than the radius of the tube. The combined use of these two approximations is called the TTTB approximation. This method does not make a distinction between standing and propagating waves. In the TTTB approximation, the period/wavelength is unaffected by the thickness of the nonuniform layer, while the temporal/spatial damping rate is linearly proportional to the thickness of the layer (e.g., Ruderman & Roberts 2002; Goossens et al. 2002; Terradas et al. 2010b). A numerical factor in the formula for the damping rate is the only remnant of the specific form of the spatial variation of density in the nonuniform layer. The use of the TT approximation is quite

reasonable in view that the magnetic waveguides in the solar atmosphere, e.g., coronal loops, chromospheric spicules, and prominence threads, are usually very thin. For instance, the geometrical properties of oscillating coronal loops reported by Aschwanden et al. (2002) indicate that oscillating loops are roughly two orders of magnitude longer than their radii. Conversely, there is no observational justification for the use of the TB approximation. The only justification for the use of the TB approximation is that it is mathematically convenient to obtain a simple analytic expression for the damping rate. Indeed, some studies suggest that coronal loops are largely inhomogeneous in the transverse direction (see, e.g., Aschwanden et al. 2003), hence the TB approximation may not be realistic.

The study of the normal modes in tubes with thick nonuniform layers requires, in general, the use of numerical computations. The inclusion of dissipation as, e.g., magnetic resistivity, is needed for the numerical schemes to properly treat the behavior of the wave perturbations across the Alfvén resonance. The effect of thick nonuniform layers was first investigated by Van Doorselaere et al. (2004), who abandoned the analytic TTTB approximation and obtained the period and damping rate of standing kink waves by means of fully numerical eigenvalue computations in resistive MHD. Later, Arregui et al. (2005) performed a similar study but including longitudinal density stratification. Resistive eigenvalue computations have been subsequently used in various studies (e.g., Terradas et al. 2006a; Arregui et al. 2008, 2011; Soler et al. 2009b,a, among others). Van Doorselaere et al. (2004) concluded that the error due to the TTTB approximation when used beyond the limit of thin layers is 25% at most. Since 25% is a relatively small error, the results of Van Doorselaere et al. (2004) support the generalization of

the TTTB approximation beyond its theoretical range of applicability. This gave rise to analytic seismological inversion schemes for kink waves that make extensive use of this approximation (Goossens et al. 2008, 2012b) and are much simpler than fully numerical inversions (Arregui et al. 2007).

In the present paper, we revisit the theoretical investigation of transverse waves in flux tubes with thick nonuniform layers. Our reasons for tackling this task are the following. (1) We aim to find an alternative method to obtain the ideal MHD modes in tubes with thick layers, which does not involve the numerical solution of resistive eigenvalues. This would remove the necessity of using resistive MHD computations. Also, the comparison of the results obtained in ideal MHD with those in resistive MHD would allow us to isolate possible effects introduced by resistivity. (2) We will investigate the kink wave eigenfunctions and energy distribution in tubes with thick layers. Van Doorselaere et al. (2004) focused on studying the period and damping rate and did not investigate the eigenfunctions. The form of the eigenfunctions is important for the spatial distribution of wave energy (Goossens et al. 2013). (3) It is likely that the form of the spatial variation of density plays a role when the nonuniform layer is thick so that most part of the tube is nonuniform. However, seismological inversion schemes based on the TTTB approximation (Goossens et al. 2008, 2012b) use an ad hoc variation of density in the nonuniform layer and ignore the influence of other density profiles. The effect of the specific transverse density variation on the accuracy of the TTTB approximation has not been determined, so that the impact of the shape of the transitional layer on seismological inversions is unknown.

To achieve the three objectives given above, we develop a general analytic method to compute the dispersion relation and the eigenfunctions of ideal MHD waves in pressureless flux tubes with transversely nonuniform layers of arbitrary thickness. The analytic process uses the Method of Frobenius to express the solution for the total pressure perturbation in the nonuniform layer as a combination of a singular and a regular series around the Alfvén resonance position. The analytic treatment is inspired by the work of Hollweg (1990b) on the absorption of MHD waves launched towards a thick Cartesian interface between two plasmas (see also Zhu & Kivelson 1988; Hollweg 1990a; Wright & Thompson 1994). The technique allows to consider any variation of density in the nonuniform layer. We investigate kink waves as an application of the method.

In this article, we are concerned with objectives (1) and (2). We present the mathematical method and compare the results in ideal MHD with those in resistive MHD. We investigate the impact of thick transitional layers on the frequency, damping rate, eigenfunctions, and energy distribution of kink waves. Objective (3) will be addressed in a forthcoming second part of this work, where we will study the effect of the shape of the transitional layer on the accuracy of the TTTB approximation and will explore the implications of the results for seismological inversions.

This article is organized as follows. Section 2 contains the description of the equilibrium configuration and the basic equations. The mathematical method is presented and explained in Section 3. Approximate results for thin nonuniform layers are obtained in Section 4. Later, general results for thick nonuniform layers are given in Section 5. The effect of the transverse density profile is investigated in Section 6. Finally, we discuss in Section 7 the theoretical and observa-

tional implications of the results.

2. MODEL AND BASIC EQUATIONS

The equilibrium configuration is made of a straight magnetic cylinder of radius R embedded in a uniform and infinite plasma. We use cylindrical coordinates, namely r , φ , and z for the radial, azimuthal, and longitudinal coordinates, respectively. The magnetic field is straight and constant and along the axis of the cylinder, namely $\mathbf{B} = B\mathbf{1}_z$. We adopt the $\beta = 0$ approximation, where β refers to the ratio of the gas pressure to the magnetic pressure. This is an appropriate approximation to describe transverse MHD waves in the solar corona. In the $\beta = 0$ approximation we can freely choose the density profile in the equilibrium state. Hence, the density, ρ , is chosen uniform in the azimuthal and longitudinal directions and nonuniform in the radial direction, namely $\rho = \rho(r)$. We consider the following profile,

$$\rho(r) = \begin{cases} \rho_i, & \text{if } r \leq R - l/2, \\ \rho_{tr}(r), & \text{if } R - l/2 < r < R + l/2, \\ \rho_e, & \text{if } r \geq R + l/2, \end{cases} \quad (1)$$

where ρ_i and ρ_e are internal and external constant densities and $\rho_{tr}(r)$ represents a density profile that continuously connects the internal plasma to the external plasma by a nonuniform transitional layer of arbitrary thickness, l . We make no assumption concerning the thickness of the transitional layer. The limit $l/R = 0$ corresponds to an abrupt jump in density, while the case $l/R = 2$ corresponds to a tube fully inhomogeneous in the radial direction. We set $\rho_i > \rho_e$ corresponding to an overdense tube with respect to the external plasma. At the present stage we do not specify the form of $\rho_{tr}(r)$.

The equilibrium magnetic flux tube described above acts as a waveguide for MHD waves. We study linear ideal MHD waves superimposed on the equilibrium state. We consider no equilibrium flows. We linearize the ideal MHD equations for a pressureless static plasma and the resulting equations are

$$\rho(r) \frac{\partial^2 \boldsymbol{\xi}}{\partial t^2} = \frac{1}{\mu} (\nabla \times \mathbf{b}) \times \mathbf{B}, \quad (2)$$

$$\mathbf{b} = \nabla \times (\boldsymbol{\xi} \times \mathbf{B}), \quad (3)$$

where $\boldsymbol{\xi} = (\xi_r, \xi_\varphi, \xi_z)$ is the plasma Lagrangian displacement, $\mathbf{b} = (b_r, b_\varphi, b_z)$ is the magnetic field perturbation, and μ is the magnetic permeability.

In the present investigation we study normal modes. The temporal dependence of perturbations is put proportional to $\exp(-i\omega t)$, with ω the frequency. In the stationary state of linear wave propagation any wavepacket can be decomposed as a sum of normal modes with different frequencies. In addition, since the equilibrium is uniform in both φ - and z -directions, we can restrict ourselves to study the individual Fourier components of the perturbations along these directions. Hence the perturbations are put proportional to $\exp(im\varphi + ik_z z)$, where m and k_z and the azimuthal and longitudinal wavenumbers, respectively. Only integer values of m are possible. Kink waves are characterized by $m = \pm 1$. From here on, we only retain the dependence of the perturbations on the radial coordinate.

Equations (2) and (3) can be combined to obtain a differential equation for the total pressure Eulerian perturbation, $P' = \mathbf{B} \cdot \mathbf{b}/\mu$, as

$$\frac{\partial^2 P'}{\partial r^2} + \left[\frac{1}{r} - \frac{\frac{d}{dr}(\rho(r)(\omega^2 - k_z^2 v_A^2(r)))}{\rho(r)(\omega^2 - k_z^2 v_A^2(r))} \right] \frac{\partial P'}{\partial r}$$

$$+ \left(\frac{\rho(r) (\omega^2 - k_z^2 v_A^2(r))}{B^2/\mu} - \frac{m^2}{r^2} \right) P' = 0, \quad (4)$$

where $v_A^2(r) = B^2/\mu\rho(r)$ is the square of the local Alfvén velocity. The radial and azimuthal components of the Lagrangian displacement, ξ_r and ξ_φ , are related to P' as

$$\xi_r = \frac{1}{\rho(r) (\omega^2 - k_z^2 v_A^2(r))} \frac{\partial P'}{\partial r}, \quad (5)$$

$$\xi_\varphi = \frac{1}{\rho(r) (\omega^2 - k_z^2 v_A^2(r))} \frac{im}{r} P'. \quad (6)$$

The longitudinal component of the Lagrangian displacement is $\xi_z = 0$ because there are no motions along the magnetic field in the $\beta = 0$ approximation.

Note in Equation (4) the presence of the term with the radial derivative of $\rho(r) (\omega^2 - k_z^2 v_A^2(r))$. This term is zero when the density, ρ , is uniform. Conversely, when ρ is nonuniform, this term causes Equation (4) to be singular at the specific position in the equilibrium, $r = r_A$, where the resonant condition $\omega^2 = k_z^2 v_A^2(r_A)$ is satisfied, with r_A denoting the Alfvén resonance position. This causes the damping of the MHD waves with $m \neq 0$.

We recall that this work is based on normal modes. It is expected that the normal modes determine the behavior of the flux tube oscillations after a transitory phase following the initial excitation (see the numerical simulations by, e.g., Terradas et al. 2006b). The resonant damping of normal modes follows an exponential law (e.g., Goossens et al. 2002; Ruderman & Roberts 2002; Terradas et al. 2010b). Recently, it has been shown in time-dependent numerical simulations that the normal mode exponential damping is preceded, in the first stages of the oscillation, by a Gaussian-like damping phase (Pascoe et al. 2012, 2013; Hood et al. 2013; Ruderman & Terradas 2013). The results discussed in this paper apply to the oscillation and damping regimes described by normal modes.

3. MATHEMATICAL METHOD

3.1. Solution in the uniform regions

In the regions with constant density Equation (4) becomes

$$\frac{d^2 P'}{dr^2} + \frac{1}{r} \frac{dP'}{dr} + \left(\frac{\omega^2 - k_z^2 v_A^2}{v_A^2} - \frac{m^2}{r^2} \right) P' = 0, \quad (7)$$

where now v_A^2 is constant. Equation (7) is the Bessel Equation. We look for solutions to Equation (7) in the internal and external plasmas. We use the subscripts ‘i’ and ‘e’ to denote quantities related to the internal and external plasmas, respectively.

In the internal plasma, i.e., $r \leq R - l/2$, we require that P' be regular at $r = 0$. Thus,

$$P'_i = A_i J_m(k_{\perp,i} r), \quad (8)$$

where A_i is a constant, J_m is the Bessel function of the first kind of order m , and

$$k_{\perp,i}^2 = \frac{\omega^2 - k_z^2 v_{A,i}^2}{v_{A,i}^2}. \quad (9)$$

We move to the external plasma, i.e., $r \geq R + l/2$. The requirement that the MHD wave is trapped in the flux tube means

that P' must vanish at $r \rightarrow \infty$. Hence, we discard leaky waves from the present investigation (see, e.g., Cally 1986, 2003). The solution to Equation (7) for $r \geq R + l/2$ is

$$P'_e = A_e K_m(k_{\perp,e} r), \quad (10)$$

where again A_e is a constant, K_m is the modified Bessel function of the first kind of order m , and

$$k_{\perp,e}^2 = -\frac{\omega^2 - k_z^2 v_{A,e}^2}{v_{A,e}^2}. \quad (11)$$

3.2. Solution in the nonuniform layer

Here we connect the solution in the internal plasma (Equation (8)) to the solution in the external medium (Equation (10)) by solving Equation (4) in the nonuniform transitional layer. We use the subscript ‘tr’ to denote quantities related to the transitional layer. The position of the Alfvén resonance, r_A , is a regular singular point. We take advantage of this fact and use the Method of Frobenius to obtain the solution to Equation (4) as an infinite power series expansion around the resonance position (see, e.g., Zhu & Kivelson 1988; Hollweg 1990b,a; Wright & Thompson 1994; Cally & Andries 2010). We assume that there is only one resonance position. The method is outlined in the following paragraphs.

We perform the change of variable

$$\zeta \equiv r - r_A. \quad (12)$$

In this new radial coordinate, the boundaries of the transitional layer are at the positions ζ_i and ζ_e , namely

$$\zeta_i = R - \frac{l}{2} - r_A, \quad (13)$$

$$\zeta_e = R + \frac{l}{2} - r_A. \quad (14)$$

We rewrite Equation (4) as

$$\zeta^2 h(\zeta) \frac{\partial^2 P'}{\partial \zeta^2} + \zeta p(\zeta) \frac{\partial P'}{\partial \zeta} + q(\zeta) P' = 0, \quad (15)$$

where the functions $h(\zeta)$, $p(\zeta)$, and $q(\zeta)$ are defined as

$$h(\zeta) = (\zeta + r_A)^2 f(\zeta), \quad (16)$$

$$p(\zeta) = \zeta (\zeta + r_A) \left[f(\zeta) - (\zeta + r_A) \frac{\partial f(\zeta)}{\partial \zeta} \right], \quad (17)$$

$$q(\zeta) = \zeta^2 \left[\frac{\mu}{B^2} (\zeta + r_A)^2 f^2(\zeta) - m^2 f(\zeta) \right], \quad (18)$$

with

$$f(\zeta) = \rho(\zeta) (\omega^2 - k_z^2 v_A^2(\zeta)) = \omega^2 \rho(\zeta) - k_z^2 \frac{B^2}{\mu}. \quad (19)$$

We assume that the density profile is an analytic function at the resonance position. Hence we perform a Taylor series of $\rho(\zeta)$ around $\zeta = 0$ as

$$\rho(\zeta) = \sum_{k=0}^{\infty} \rho_k \zeta^k, \quad (20)$$

with $\rho_0 = \rho(\zeta = 0) = \rho(r = r_A)$ and

$$\rho_k = \frac{1}{k!} \left. \frac{d^k \rho(\zeta)}{d\zeta^k} \right|_{\zeta=0} = \frac{1}{k!} \left. \frac{d^k \rho(r)}{dr^k} \right|_{r=r_A}, \quad \text{for } k \geq 1. \quad (21)$$

Note that we do not specify the form of the density profile, $\rho(r)$. We recall that the only requirements are, first, that the density profile is an analytic function at $r = r_A$ and, second, that there is only one resonance position. The analysis below is valid for any density profile satisfying these two conditions.

We express the solution to Equation (15) in the form of series expansion around the regular singular point $\zeta = 0$, namely

$$P'_{\text{tr}}(\zeta) = \zeta^s \sum_{k=0}^{\infty} a_k \zeta^k \quad (22)$$

where s is the index of the expansion and a_k are coefficients to be determined. The value of the coefficients a_k depend on the specific density profile considered. We substitute Equation (22) in Equation (15). The relation determining the values of the index s is obtained from the coefficient of the lowest power of ζ in the resulting infinite series. This leads to the indicial equation $s(s-2) = 0$, with roots $s_1 = 2$ and $s_2 = 0$ (see also Goossens et al. 1992). Then, the general solution to Equation (15) is the sum of two linearly independent solutions, namely a regular series, $P'_1(\zeta)$, and a singular series, $P'_2(\zeta)$. The expressions of this two linearly independent solutions are

$$P'_1(\zeta) = \zeta^2 \sum_{k=0}^{\infty} a_k \zeta^k, \quad (23)$$

$$P'_2(\zeta) = \sum_{k=0}^{\infty} s_k \zeta^k + CP'_1(\zeta) \ln \zeta, \quad (24)$$

where C is the coupling constant and a_k and s_k are series coefficients. The general solution to Equation (15) is then

$$P'_{\text{tr}}(\zeta) = A_0 P'_1(\zeta) + S_0 P'_2(\zeta), \quad (25)$$

where A_0 and S_0 are constants. Since the general solution to a 2nd order ordinary differential equation contains two undetermined coefficients, we adopt $a_0 = s_0 = 1$ with no loss of generality. The expressions of the remaining coefficients a_k and s_k and that of the coupling constant C are obtained after substituting Equation (25) in Equation (15). The coefficients a_k and s_k depend on the choice of the density profile, but the coupling constant is independent of the density profile, namely

$$C = \frac{m^2}{2r_A^2}. \quad (26)$$

When $m = 0$, $C = 0$ and the singular series, $P'_2(\zeta)$, becomes a regular series due to the absence of the logarithmic term. As a consequence, no resonance takes place when $m = 0$. General expressions of the coefficients a_k and s_k and their recurrence relations are given in the Appendix.

Finally, the expressions of ξ_r and ξ_φ in the transitional layer are straightforwardly obtained by substituting Equation (25) in Equations (5) and (6), respectively.

3.3. Dispersion relation

The dispersion relation is obtained by imposing the continuity of P' and ξ_r at $r = R - l/2$ and $r = R + l/2$. These boundary conditions provide us with a system of four algebraic equations for the constants A_i , A_e , A_0 , and S_0 . The requirement that there is a nontrivial solution of the system provides us with the dispersion relation. For simplicity, we

omit the intermediate steps and give the final expression of the dispersion relation, namely

$$\frac{\frac{k_{\perp,e}}{\rho_e(\omega^2 - k_z^2 v_{A,e}^2)} \frac{K'_m[k_{\perp,e}(R+l/2)]}{K_m[k_{\perp,e}(R+l/2)]} \mathcal{G}_e - \Xi_e}{\frac{k_{\perp,e}}{\rho_e(\omega^2 - k_z^2 v_{A,e}^2)} \frac{K'_m[k_{\perp,e}(R+l/2)]}{K_m[k_{\perp,e}(R+l/2)]} \mathcal{F}_e - \Gamma_e} - \frac{\frac{k_{\perp,i}}{\rho_i(\omega^2 - k_z^2 v_{A,i}^2)} \frac{J'_m[k_{\perp,i}(R-l/2)]}{J_m[k_{\perp,i}(R-l/2)]} \mathcal{G}_i - \Xi_i}{\frac{k_{\perp,i}}{\rho_i(\omega^2 - k_z^2 v_{A,i}^2)} \frac{J'_m[k_{\perp,i}(R-l/2)]}{J_m[k_{\perp,i}(R-l/2)]} \mathcal{F}_i - \Gamma_i} = 0, \quad (27)$$

where

$$\mathcal{G}_{i,e} = \sum_{k=0}^{\infty} a_k \zeta_{i,e}^{k+2}, \quad (28)$$

$$\mathcal{F}_{i,e} = \sum_{k=0}^{\infty} \left(s_k \zeta_{i,e}^k + \frac{m^2}{2r_A^2} \ln(\zeta_{i,e}) a_k \zeta_{i,e}^{k+2} \right), \quad (29)$$

$$\Xi_{i,e} = \frac{1}{\omega^2 \sum_{k=0}^{\infty} \rho_{k+1} \zeta_{i,e}^k} \sum_{k=0}^{\infty} (k+2) a_k \zeta_{i,e}^k, \quad (30)$$

$$\Gamma_{i,e} = \frac{1}{\omega^2 \sum_{k=0}^{\infty} \rho_{k+1} \zeta_{i,e}^k} \sum_{k=0}^{\infty} \left(k s_k \zeta_{i,e}^{k-2} + \frac{m^2}{2r_A^2} a_k \zeta_{i,e}^k + \frac{m^2}{2r_A^2} \ln(\zeta_{i,e}) (k+2) a_k \zeta_{i,e}^k \right). \quad (31)$$

Equation (27) is valid for any value of m , namely $m = 0$ sausage modes, $m = 1$ kink modes, and $m \geq 2$ fluting modes. When $m \neq 0$, the dispersion relation is a multivalued function due to the presence of logarithmic terms. To make the dispersion relation univalued when $m \neq 0$, the branch points of the logarithm functions are connected in the complex plane with appropriate branch cuts (see details in, e.g., Tataronis & Grossmann 1973; Goedbloed & Poedts 2004). The dispersion relation has no solutions on the principal Riemann sheet because, strictly speaking, complex eigenvalues are not possible in ideal MHD (Poedts & Kerner 1991; Goedbloed & Poedts 2004). To find the physical solutions that represent damped waves, we have to consider the analytic continuation of the dispersion relation to the next Riemann sheet (see, e.g., Sedláček 1971). The logarithmic terms are absent when $m = 0$, so that the dispersion relation is univalued and there is no resonant damping in that case.

We recall that neither the form of the density variation nor the thickness of the non-uniform layer have been imposed so far. Equation (27) is the valid dispersion relation for any density profile and for $l/R \in (0, 2)$. The form of the density profile only affects the values of the coefficients in $\mathcal{G}_{i,e}$, $\mathcal{F}_{i,e}$, $\Xi_{i,e}$, and $\Gamma_{i,e}$.

Also, note that the present formalism is the same for both standing and propagating waves. The dispersion relation (Equation (27)) is the same in both cases. Standing waves are described by a real k_z , so that the solution of Equation (27) is a complex frequency, namely $\omega = \omega_R + i\omega_I$, where ω_R and ω_I are the real and imaginary parts of ω , respectively. Due to resonant damping $\omega_I < 0$ and, because of the temporal dependence $\exp(-i\omega t)$, the amplitude of the waves decreases in time by the exponential factor $\exp(-|\omega_I| t)$. Conversely propagating waves are described by a real ω , so that the solution of the dispersion relation is a complex longitudinal wavenumber, namely $k_z = k_{z,R} + ik_{z,I}$, where $k_{z,R}$ and $k_{z,I}$ are the real and

imaginary parts of k_z , respectively, and $k_{z,I} > 0$. The amplitude of the propagating waves decreases in z by the exponential factor $\exp(-k_{z,I}z)$. Therefore, standing and propagating cases are equivalent and are both described by the same dispersion relation (Equation (27)).

4. APPROXIMATE RESULTS FOR THIN LAYERS

In general, for arbitrary values of l/R , Equation (27) has to be solved numerically. However, analytic approximations to the solutions with $m \neq 0$ can be obtained when l/R is a small parameter and only the leading terms in the expressions of $\mathcal{G}_{i,e}$, $\mathcal{F}_{i,e}$, $\Xi_{i,e}$, and $\Gamma_{i,e}$ are retained. We assume that the nonuniform layer is sufficiently thin so that it suffices to keep terms up to $O(l/R)$. A similar situation has been previously studied by, e.g., Goossens et al. (1992, 2002); Ruderman & Roberts (2002) for standing waves and by Terradas et al. (2010b) for propagating waves using the TB approximation, i.e., $l/R \ll 1$. Before tackling the general study for arbitrary l/R , the purpose of this Section is to recover with the present formalism the known results in the TB limit. This is useful to check the validity of the Frobenius method.

4.1. Solution to the dispersion relation

By retaining terms up to $O(l/R)$ only, the expressions of $\mathcal{G}_{i,e}$, $\mathcal{F}_{i,e}$, $\Xi_{i,e}$, and $\Gamma_{i,e}$ reduce to

$$\mathcal{G}_{i,e} \approx 0, \quad (32)$$

$$\mathcal{F}_{i,e} \approx 1, \quad (33)$$

$$\Xi_{i,e} \approx \frac{2}{\omega^2 \rho_i} = \frac{2}{\omega^2 (d\rho/dr)_R}, \quad (34)$$

$$\Gamma_{i,e} \approx \frac{m^2/R^2}{\omega^2 \rho_i} \left(\ln \zeta_{i,e} + \frac{1}{2} \right) = \frac{m^2/R^2}{\omega^2 (d\rho/dr)_R} \left(\ln \zeta_{i,e} + \frac{1}{2} \right), \quad (35)$$

where we took $r_A \approx R$ as consistent with the assumption that the layer is thin so that the resonance position is close to $r = R$. We approximate $\mathcal{G}_{i,e} \approx 0$ because the first nonzero terms in $\mathcal{G}_{i,e}$ are of $O(l/R)^2$. Then, the dispersion relation (Equation (27)) becomes

$$\frac{k_{\perp,e}}{\rho_e (\omega^2 - k_z^2 v_{A,e}^2)} \frac{K'_m(k_{\perp,e}R)}{K_m(k_{\perp,e}R)} - \frac{k_{\perp,i}}{\rho_i (\omega^2 - k_z^2 v_{A,i}^2)} \frac{J'_m(k_{\perp,i}R)}{J_m(k_{\perp,i}R)} = \frac{m^2/R^2}{\omega^2 (d\rho/dr)_R} \ln \left(\frac{\zeta_e}{\zeta_i} \right), \quad (36)$$

where we used $R - l/2 \approx R + l/2 \approx R$ as consistent with the thin layer assumption. Equation (36) is valid for arbitrary values of $k_z R$ because no restriction has been imposed on the radius of the magnetic tube. When $l = 0$, $(d\rho/dr)_R \rightarrow \infty$ and the right-hand side of Equation (36) vanishes. Then, the dispersion relation simplifies to

$$\frac{k_{\perp,e}}{\rho_e (\omega^2 - k_z^2 v_{A,e}^2)} \frac{K'_m(k_{\perp,e}R)}{K_m(k_{\perp,e}R)} - \frac{k_{\perp,i}}{\rho_i (\omega^2 - k_z^2 v_{A,i}^2)} \frac{J'_m(k_{\perp,i}R)}{J_m(k_{\perp,i}R)} = 0, \quad (37)$$

Equation (37) is the well-known dispersion relation of Edwin & Roberts (1983). To obtain an analytic approximation for kink waves we consider the TT approximation and take the limit $k_z R \ll 1$. We use an asymptotic expansion for

small arguments and $m \neq 0$ of the Bessel functions in Equation (37) and keep the first term in the expansions, so that we approximate

$$\frac{J'_m(k_{\perp,i}R)}{J_m(k_{\perp,i}R)} \approx \frac{m}{k_{\perp,i}R}, \quad \frac{K'_m(k_{\perp,e}R)}{K_m(k_{\perp,e}R)} \approx -\frac{m}{k_{\perp,e}R}. \quad (38)$$

Equation (37) simplifies to

$$\rho_i (\omega^2 - k_z^2 v_{A,i}^2) + \rho_e (\omega^2 - k_z^2 v_{A,e}^2) = 0. \quad (39)$$

For standing waves, k_z is fixed and ω is given by the solution of Equation (39), namely

$$\omega^2 = \frac{\rho_i v_{A,i}^2 + \rho_e v_{A,e}^2}{\rho_i + \rho_e} k_z^2 = \frac{2B^2/\mu}{\rho_i + \rho_e} k_z^2 \equiv \omega_k^2. \quad (40)$$

ω_k is real and is called the kink frequency (see, e.g., Edwin & Roberts 1983; Goossens et al. 2009). Conversely, for propagating waves ω is fixed and k_z is given by the solution of Equation (39), namely

$$k_z^2 = \frac{\rho_i + \rho_e}{\rho_i v_{A,i}^2 + \rho_e v_{A,e}^2} \omega^2 = \frac{\rho_i + \rho_e}{2B^2/\mu} \omega^2 \equiv k_{z,k}^2, \quad (41)$$

where $k_{z,k}$ can be equivalently called the kink wavenumber.

We go back to the general case with $l \neq 0$. To evaluate the logarithmic term on the right-hand side of Equation (36), we realize that assuming $r_A \approx R$ results in $\zeta_i \approx -l/2$ and $\zeta_e \approx l/2$, and we define the complex logarithm so that it jumps $\pm i\pi$ when crossing the negative real axis. Accordingly we approximate $\ln(\zeta_e/\zeta_i) \approx \pm i\pi$, where either the + sign or the - sign is conveniently chosen depending on the sign of $(\partial\rho/\partial r)_R$. This choice is based on the physical argument that the effect of the resonance is to produce the damping of the waves. As in the case with $l = 0$, in order to make further analytic progress we consider the TT approximation, $k_z R \ll 1$, and expand the Bessel functions for small arguments. Equation (36) reduces to

$$\rho_i (\omega^2 - k_z^2 v_{A,i}^2) + \rho_e (\omega^2 - k_z^2 v_{A,e}^2) - i\pi \frac{m}{R} \frac{\rho_i \rho_e}{|d\rho/dr|_R} \frac{(\omega^2 - k_z^2 v_{A,i}^2)(\omega^2 - k_z^2 v_{A,e}^2)}{\omega^2} = 0. \quad (42)$$

Equation (42) agrees with the dispersion relation derived by Goossens et al. (1992) in the TT and TB limits. The joint use of the TT and TB approximations is called here the TTTB approximation.

Let us first study standing waves. To find an analytic approximation to the kink mode frequency, we write $\omega = \omega_R + i\omega_I$ and fix k_z to a real value. We assume weak damping, i.e., $\omega_I^2 \ll \omega_R^2$, so that we neglect terms with ω_I^2 and higher powers in Equation (42). The real part of the frequency, ω_R , is approximately obtained by setting the real part of Equation (42) to zero and substituting ω^2 by ω_R^2 . Hence we obtain

$$\omega_R \approx \omega_k, \quad (43)$$

where ω_k is given in Equation (40). The wave period, P , is

$$P = \frac{2\pi}{\omega_k}. \quad (44)$$

According to Equations (43) and (44), the kink wave frequency, and so the period, is unaffected by the thickness of the transitional layer in the first-order approximation. The same expression as for $l = 0$ is found.

The approximation for ω_1 is obtained using the expression

$$\omega_1 \approx - \frac{D_I}{\partial D_R / \partial \omega} \Big|_{\omega \approx \omega_R}, \quad (45)$$

where D_R and D_I are the real and imaginary parts of the dispersion relation (Equation (42)), respectively. After some algebraic manipulations the result is

$$\omega_1 \approx - \frac{\pi m (\rho_i - \rho_e)^2}{8 R \rho_i + \rho_e} \frac{\omega_k}{|d\rho/dr|_R}. \quad (46)$$

Now we express

$$\left| \frac{d\rho}{dr} \right|_R = F \frac{\pi^2}{4} \frac{\rho_i - \rho_e}{l}, \quad (47)$$

where we introduce the numerical factor F that depends on the specific form of the density profile. For example, $F = 4/\pi^2$ for a linear variation of density and $F = 2/\pi$ for a sinusoidal variation of density. Using Equation (47) in Equation (46) we obtain

$$\omega_1 \approx - \frac{m}{2\pi F} \frac{l}{R} \frac{\rho_i - \rho_e}{\rho_i + \rho_e} \omega_k. \quad (48)$$

Equation (48) is the same damping rate found previously by, e.g., Goossens et al. (1992, 2002) for a linear density profile and by Ruderman & Roberts (2002) for a sinusoidal density profile. Equation (48) is also equivalent to the damping rate found by, e.g., Sedláček (1971); Ionson (1978); Lee & Roberts (1986); Hollweg & Yang (1988) for a surface wave in a Cartesian interface with a linear density profile, where m/R has to be replaced by the component of the wavevector in the direction perpendicular to both the interface and the density gradient.

We compute the damping time as $\tau_D = 1/|\omega_1|$ and use Equations (44) and (48) to give the expression of the ratio of the damping time to the period, namely

$$\frac{\tau_D}{P} = \frac{F R \rho_i + \rho_e}{m l \rho_i - \rho_e}. \quad (49)$$

In summary, Equation (43) shows that the kink wave frequency is independent of l/R , whereas Equation (48) predicts a linear dependence of the damping rate with l/R , so that the larger l/R , the stronger the damping. The factor F is the only remnant of the form of the density profile that remains in the TTTB formula. Apart from this numerical factor, the dependence of τ_D/P with l/R is not affected by the form of the density profile in the thin nonuniform layer limit (Equation (49)).

Now, we turn to propagating waves. We write $k_z = k_{z,R} + ik_{z,I}$ and fix ω to a real value. Following the same process as before, we find the approximations to $k_{z,R}$ and $k_{z,I}$ as

$$k_{z,R} \approx k_{z,k}, \quad (50)$$

$$k_{z,I} \approx \frac{m}{2\pi F} \frac{l}{R} \frac{\rho_i - \rho_e}{\rho_i + \rho_e} k_{z,k}, \quad (51)$$

which agree with the expressions found by Terradas et al. (2010b). We compute the ratio of the damping length, $L_D = 1/k_{z,I}$, to the wavelength, $\lambda = 2\pi/k_{z,R}$, as

$$\frac{L_D}{\lambda} = \frac{F R \rho_i + \rho_e}{m l \rho_i - \rho_e}, \quad (52)$$

which is exactly the same expression as for the standing waves τ_D/P (Equation (49)). In both standing and propagating cases

the Frobenius method is consistent with the approximations found in previous works when the TT ($k_z R \ll 1$) and TB ($l/R \ll 1$) limits are taken in the general dispersion relation.

4.2. Eigenfunctions and radial energy flux

Approximations to the eigenfunctions of P' , ξ_r , and ξ_φ in the case of an abrupt jump in density were obtained in the TT limit by, e.g., Dymova & Ruderman (2006) Goossens et al. (2009). In the regions with constant density, we follow these previous works and perform asymptotic expansions for small arguments and $m \neq 0$ of Equations (8) and (10). In the thin nonuniform layer, we only keep terms up to $O(l/R)$ in the general expression of P'_{tr} (Equation (25)). Hence, the approximation to P' is

$$P'(r) \approx \begin{cases} S_0 \frac{l}{R}, & \text{if } r \leq R - l/2, \\ S_0, & \text{if } R - l/2 < r < R + l/2, \\ S_0 \frac{R}{r}, & \text{if } r \geq R + l/2, \end{cases} \quad (53)$$

The value of P' in the thin transitional layer is constant (Hollweg & Yang 1988). In turn, the approximations for the Lagrangian displacements ξ_r and ξ_φ up to $O(l/R)$ are

$$\xi_r(r) \approx \begin{cases} D, & \text{if } r \leq R - l/2, \\ D + \frac{m^2}{R^2} \frac{S_0}{\omega^2 (d\rho/dr)_R} \ln \frac{r-r_A}{R-r_A-l/2}, & \text{if } R - l/2 < r < R + l/2, \\ D \left(\frac{R}{r} \right)^2, & \text{if } r \geq R + l/2, \end{cases} \quad (54)$$

and

$$\xi_\varphi(r) \approx \begin{cases} imD, & \text{if } r \leq R - l/2, \\ \frac{im}{R} \frac{S_0}{\omega^2 (d\rho/dr)_R} \frac{1}{r-r_A}, & \text{if } R - l/2 < r < R + l/2, \\ -imD \left(\frac{R}{r} \right)^2, & \text{if } r \geq R + l/2, \end{cases} \quad (55)$$

where

$$D = \frac{1}{\rho_i (\omega^2 - k_z^2 v_{A,i}^2)} \frac{S_0}{R} = - \frac{1}{\rho_e (\omega^2 - k_z^2 v_{A,e}^2)} \frac{S_0}{R}. \quad (56)$$

We obtain that ξ_r has a logarithmic jump at $r = r_A$, while ξ_φ behaves as $\xi_\varphi \sim (r - r_A)^{-1}$ in the transitional layer. This implies that the dominant dynamics in the vicinity of the resonance is contained in the azimuthal component or, in a general geometry, the component in the magnetic surfaces perpendicular to the magnetic field lines (see, e.g., Goedbloed 1983).

We define the variation of the quantity X across the transitional layer as

$$[X] = X_e - X_i, \quad (57)$$

where $X_{e,i}$ denote the value of X at $r = R \pm l/2$, respectively. Thus the variation of P' and ξ_r across the thin transitional layer is

$$[P'] = P'_{tr}(R + l/2) - P'_{tr}(R - l/2) \approx 0, \quad (58)$$

$$[\xi_r] = \xi_{r,tr}(R + l/2) - \xi_{r,tr}(R - l/2) \approx \frac{m^2}{R^2} \frac{S_0}{\omega^2 (d\rho/dr)_R} \ln \frac{\zeta_e}{\zeta_i}$$

$$\approx -i\pi \frac{m^2/R^2}{\omega^2 |d\rho/dr|_R} P'(R). \quad (59)$$

The variation of P' and ξ_r across a thin nonuniform layer obtained with the present method coincide with the relations derived by, e.g., Sakurai et al. (1991), for the jump of the eigenfunctions across the resonant layer in the presence of dissipation. These jump relations appear naturally in ideal MHD with the Frobenius method. In the specific case with $l = 0$,

both P' and ξ_r are continuous at $r = R$, while only ξ_φ jumps at the boundary so that $\xi_{\varphi,i} = -\xi_{\varphi,e}$ at $r = R$.

The finite jumps of the eigenfunctions in the nonuniform layer are mathematically caused by the logarithmic term in the singular Frobenius series. The physical reason for the existence of these jumps is that there is a net flux of energy toward the nonuniform layer from both sides, which is the ultimate cause of the kink wave damping. The expression of the radial component of the time-averaged energy flux is (e.g., Bray & Loughhead 1974; Stenuit et al. 1999; Arregui et al. 2011; Goossens et al. 2013)

$$\langle S_r \rangle = -\frac{1}{2} \text{Re}(i\omega \xi_r P'^*), \quad (60)$$

where the asterisk denotes the complex conjugate. We use Equations (58) and (59) to compute the jump of $\langle S_r \rangle$ as

$$[\langle S_r \rangle] \approx -\frac{\pi}{2} \frac{m^2/R^2}{\omega_R |d\rho/dr|_R} P'^2(R). \quad (61)$$

This expression is in agreement with Andries et al. (2000). Since $[\langle S_r \rangle] < 0$, the energy inflow into the resonance from the flux tube interior is larger than the energy inflow from the external plasma. When $l = 0$, $\langle S_r \rangle = 0$ so that there is no radial flux of energy.

5. RESULTS FOR THICK LAYERS

In Section 4 we showed that the solutions obtained with the Frobenius method consistently revert to the approximations found in previous works when the TTTB limit is considered. Here, we go beyond the limitation of the TTTB approximation. We fully exploit the Frobenius method by considering arbitrary values of the ratio l/R . We solve the general dispersion relation (Equation (27)) to compute the frequency and damping rates beyond the case of thin layers. The dispersion relation is a transcendental equation whose roots are found by standard numerical methods. The expressions of $\mathcal{G}_{i,e}$, $\mathcal{F}_{i,e}$, $\Xi_{i,e}$, and $\Gamma_{i,e}$ involve series with infinite number of terms. To proceed numerically we must truncate the infinite series so that only the first N terms are accounted for. To make sure that the number of terms considered is large enough for the error to be negligible, we perform convergence tests by increasing N until a good convergence of the solution to Equation (27) is obtained. Typically, we take $N = 51$.

In addition to the ideal normal modes obtained with the Frobenius method, we consider the numerical solution of the resistive eigenvalue problem with the PDE2D code (Sewell 2005). This is the same approach used by Van Doorselaere et al. (2004), although here we perform the computations with a different numerical code. This will allow us to compare the results in ideal MHD with those in resistive MHD. In the numerical code, the magnetic diffusion term, $\eta \nabla^2 \mathbf{b}$, is included in the right-hand side of the linearized induction equation (Equation (3)), where η is the coefficient of magnetic resistivity. We take η as a constant for simplicity. We define the magnetic Reynolds number as $R_m = v_{A,i} R / \eta$. In the solar corona $R_m \sim 10^{12}$ because η is extremely small. Using a realistic value for R_m requires taking an enormous number of grid points in the numerical domain. This is not practical from the computational point of view. Therefore, we use in our computations a smaller value of R_m . We take values of R_m in between 10^5 – 10^7 . This is computationally advantageous because we can take a smaller

number of grid points. However, although in our computations R_m is smaller than its realistic value, we make sure that R_m is still large enough for resistive damping to be negligible compared to resonant damping. In other words, resistivity has no impact on the wave frequency and damping rate (see, e.g., Poedts & Kerner 1991; Van Doorselaere et al. 2004; Terradas et al. 2006a). The PDE2D code solves the resistive eigenvalue problem using a finite-element scheme in a nonuniform grid. The numerical integration of the resistive MHD equations is performed from the cylinder axis, $r = 0$, to the edge of the numerical domain, $r = r_{\max}$. We take $r_{\max} \gg R$ to avoid numerical errors and to obtain a good convergence of the solution. The PDE2D code uses a collocation method and the generalized matrix eigenvalue problem is solved using the shifted inverse power method. The output of the program is the closest complex eigenvalue to the initial provided guess and the corresponding eigenfunctions.

Since standing and propagating waves are equivalent from the mathematical point of view, from here on we focus on standing waves. We introduce the parameter L that represents the length of the magnetic flux tube. Standing waves whose perturbations are line-tied at the ends of the flux tube are characterized by quantized values of k_z given by

$$k_z = \frac{n\pi}{L}, \quad (62)$$

where $n = 1$ for the fundamental mode, $n = 2$ for the first overtone, and so on. We restrict ourselves to the fundamental kink mode, so we take $n = 1$ and $m = 1$. In this Section, we assume a sinusoidal variation for the density in the nonuniform layer, namely

$$\rho_{tr}(r) = \frac{\rho_i}{2} \left[\left(1 + \frac{\rho_e}{\rho_i} \right) - \left(1 - \frac{\rho_e}{\rho_i} \right) \sin \left(\frac{\pi}{l}(r - R) \right) \right]. \quad (63)$$

This is the same density profile used in the computations by Van Doorselaere et al. (2004). On purpose, we choose this density profile to compare our results with those reported in this previous work. Other equilibrium density profiles are considered in Section 6.

5.1. Frequency and damping rate

Figure 1 displays the real and imaginary parts of the fundamental kink mode frequency versus l/R for a tube with $L/R = 100$ and four different values of the density contrast, ρ_i/ρ_e . The solid lines correspond to the results of the ideal Frobenius method.

Regarding the real part of the frequency (Figure 1(a)), we find that $\omega_R \approx \omega_k$ is a reasonably good approximation up to $l/R \approx 1$. For thicker layers, the real part of the kink wave frequency increases and becomes larger than ω_k . This result is in agreement with Figure 8 of Van Doorselaere et al. (2004). It is also consistent with Figure 5(a) of Arregui et al. (2005) with their stratification parameter set to $\alpha = 0$. Although it depends on the density contrast, the actual ω_R is around 15% larger than ω_k when $l/R \approx 2$.

We turn to the imaginary part of the frequency (Figure 1(b)). Visually, we see that the TTTB formula (Equation (48)) provides a good approximation to the damping rate when $l/R \lesssim 0.4$. For thicker layers, the full result deviates from the linear dependence predicted in the TTTB approximation. In addition, we find that beyond the limit of thin layers the density contrast has an impact on the shape of the curves, so that the curves of ω_i obtained for different ρ_i/ρ_e do

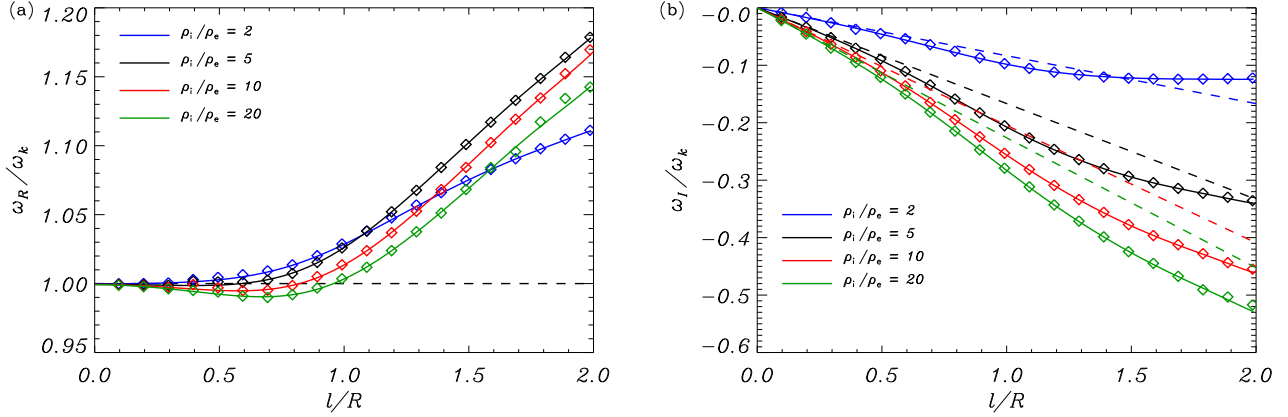


Figure 1. (a) Real part and (b) imaginary part of the kink mode frequency versus l/R . In both panels the solid lines correspond to the solutions of the ideal dispersion relation (Equation (27)), the dashed lines are the TTTB analytic results (Equations (43) and (48)), and the symbols are the resistive MHD eigenvalue results obtained with the PDE2D code. The line color denotes the value of ρ_i/ρ_e used in the computation (indicated within the figures). In all cases we use a sinusoidal transition of density and $L/R = 100$.

not show the same dependence with l/R . This dependence of the damping rate with the density contrast is not captured by the TTTB formula. For example, the curve with $\rho_i/\rho_e = 2$ in Figure 1(b) saturates on a certain value and intersects the thin layer solution when $l/R \approx 1.5$. This behavior can also be seen in Figures 4 and 5 of Van Doorselaere et al. (2004). Conversely, the rest of curves in Figure 1(b) corresponding to larger contrasts do not reach a saturation value and do not intersect the TTTB solution (see also Van Doorselaere et al. 2004, Fig. 11). In those cases the TTTB formula underestimates the actual damping rate. The largest deviation from the TTTB values takes place at $l/R \approx 1$, where the error done due to the TTTB approximation is around 25%. Again, these results are in good agreement with Van Doorselaere et al. (2004).

To further check the results discussed above, we repeat the computations of the frequency and damping rate with the resistive MHD code using the same parameters as in Figure 1. The resistive results are overplotted in Figure 1 with the symbol \diamond . We find an excellent agreement between the ideal results obtained using the Frobenius method and the resistive MHD computations. This fact makes us confident that the analytic Frobenius method gives correct results. We do not need to use the more computationally expensive resistive MHD computations to find the kink mode frequency and damping rate for thick transitional layers.

5.2. Eigenfunctions

This Subsection contains information on the eigenfunctions computed, on the one hand, with the use of the ideal MHD equations and the Frobenius method and, on the other hand, with the use of the resistive MHD equations. The eigenfunctions were not discussed in the paper by Van Doorselaere et al. (2004).

We plot in Figure 2 the ideal eigenfunctions P' , ξ_r , and ξ_φ as functions of r/R for an equilibrium flux tube with $l/R = 0.2$. The behavior of the eigenfunctions in the nonuniform layer is well described by the analytic TTTB approximations of Section 4.2. Hence, P' is almost constant, $\text{Im}(\xi_r)$ has a logarithmic jump, and ξ_φ varies as $(r - r_A)^{-1}$ near the resonance position. For comparison, we also display in Figure 2 the resistive eigenfunctions obtained with the PDE2D code. The agreement between the ideal eigenfunctions and the resistive

eigenfunctions is very good. The only noticeable differences are at the center of the nonuniform layer, close to the resonance position. There, the amplitude of $\text{Re}(\xi_r)$ is slightly larger in the resistive case than in the ideal case, and the resistive ξ_φ displays some spatial oscillations not present in its ideal counterpart. The total pressure perturbation, P' , is identical in both cases.

We increase the thickness of the nonuniform layer and set $l/R = 1.5$. We are outside the range of validity of the TTTB approximation. We display in Figure 3 the ideal and resistive eigenfunctions corresponding to this case and notice that there are significant differences. All the ideal eigenfunctions jump at the resonance position, including P' . The approximation that P' is constant across the resonance (e.g., Hollweg & Yang 1988; Sakurai et al. 1991) is not satisfied for thick layers. The constancy of P' is only approximately valid when the damping is weak so that $\omega_1^2 \ll \omega_R^2$, as happens for thin layers. The jumps in the resistive version of P' are smoothed due to the effect of resistivity. The most significant differences appear when comparing the ideal and resistive components of the Lagrangian displacement. The amplitudes of the resistive ξ_r and ξ_φ are, approximately, 10 times larger and 100 times larger, respectively, than their ideal counterparts and display spatial oscillations in the nonuniform layer instead of the jumps seen in the ideal eigenfunctions. Outside the dissipative layer the amplitudes of the resistive ξ_r and ξ_φ are negligible.

The different behavior of ideal and resistive eigenfunctions was discussed by Poedts & Kerner (1991). Although they considered another equilibrium, the results of Poedts & Kerner (1991) can be directly related to the present study. Poedts & Kerner (1991) found that the ideal normal mode frequencies are correctly recovered from the resistive eigenvalues in the limit of small resistivity. This is also the case here, because the frequency and damping rate obtained with the ideal Frobenius method fully agree with the resistive eigenvalues (see Figure 1). However, Poedts & Kerner (1991) found that the resistive eigenfunctions do not converge to their ideal counterparts in the limit of small resistivity. Instead, the spatial oscillations of the resistive eigenfunctions get confined to a thinner and thinner region as η decreases. In the stationary case, i.e., for $\omega_1 = 0$, the spatial oscillations in the resistive eigenfunctions are confined to a region surrounding the resonance position, i.e., the dissipative layer. The thickness of

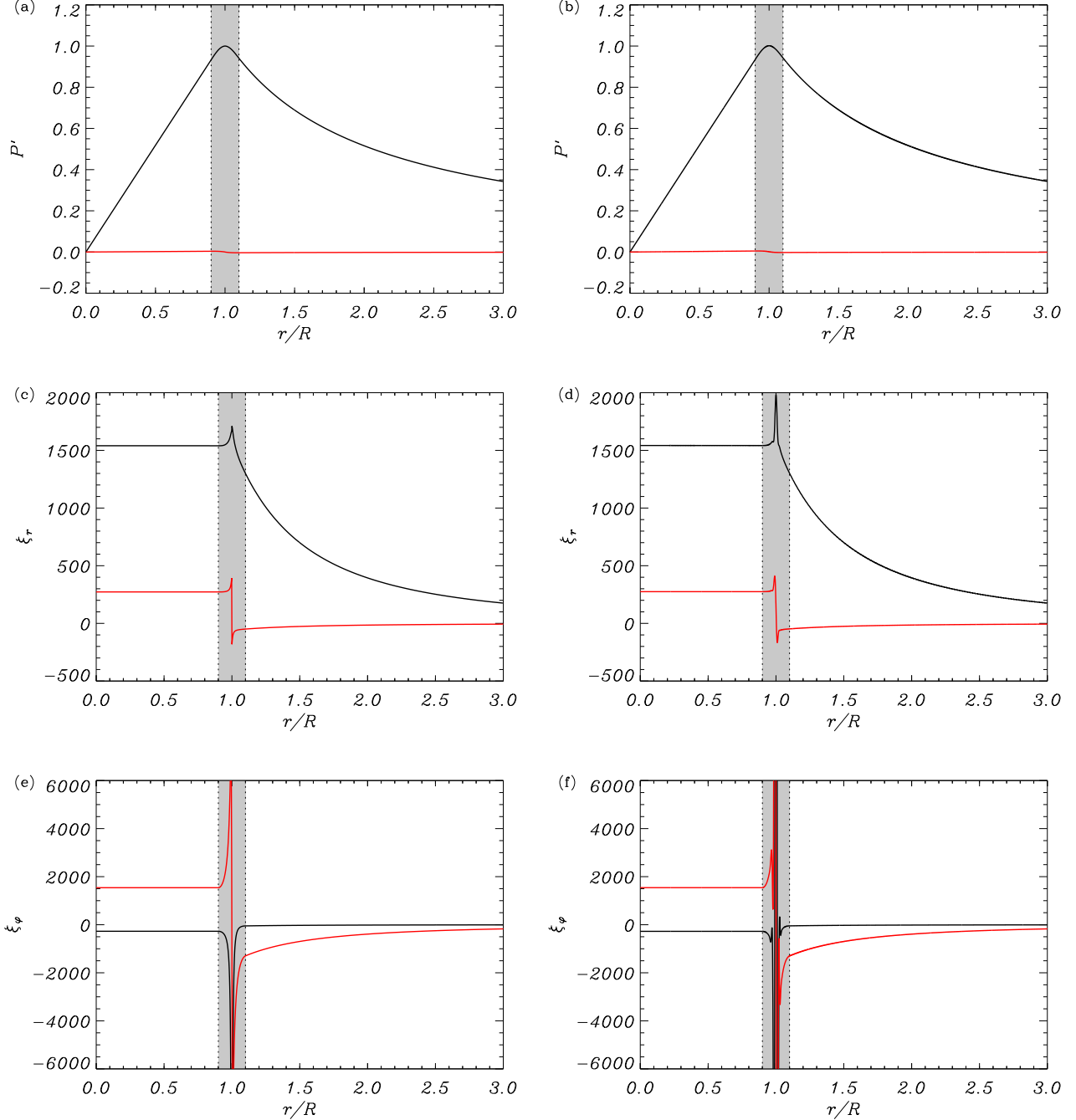


Figure 2. Kink mode eigenfunctions P' (top), ξ_r (mid), and ξ_ϕ (bottom) as functions of r/R for $l/R = 0.2$. Left panels are the ideal MHD eigenfunctions obtained with the Frobenius method, whereas the right panels are the resistive eigenfunctions computed with the PDE2D code. The black and red colors correspond to the real and imaginary parts of the eigenfunction, respectively. The shaded area denotes the nonuniform layer. Arbitrary units are used so that $\max[\text{Re}(P')]=1$. We use a sinusoidal transition of density, $L/R = 100$, and $\rho_i/\rho_e = 5$.

the dissipative layer is measured by the quantity δ_A (see, e.g., Sakurai et al. 1991)

$$\delta_A = \left(\frac{\omega_R \eta}{|\Delta_A|} \right)^{1/3}, \quad (64)$$

where $\Delta_A = \frac{d}{dr}(\omega^2 - k_z^2 v_A^2)|_{r_A}$. The dissipative layer covers the interval $r \in [r_A - \epsilon \delta_A, r_A + \epsilon \delta_A]$ with $\epsilon \approx 5$ (Goossens et al. 1995). In addition, for the damped modes of interest here, i.e., for $\omega_I < 0$, there is another length scale that determines the

spatial extent of the oscillations around the resonance. This length scale due to nonstationarity, δ_{NS} , is given by (e.g., Ruderman et al. 1995; Andries 2003)

$$\delta_{NS} = \left| \frac{2\omega_R \omega_I}{\Delta_A} \right|. \quad (65)$$

Due to the effect of nonstationarity, the oscillatory domain around the resonance does not keep decreasing indefinitely when η is decreased (Ruderman et al. 1995). Instead, the

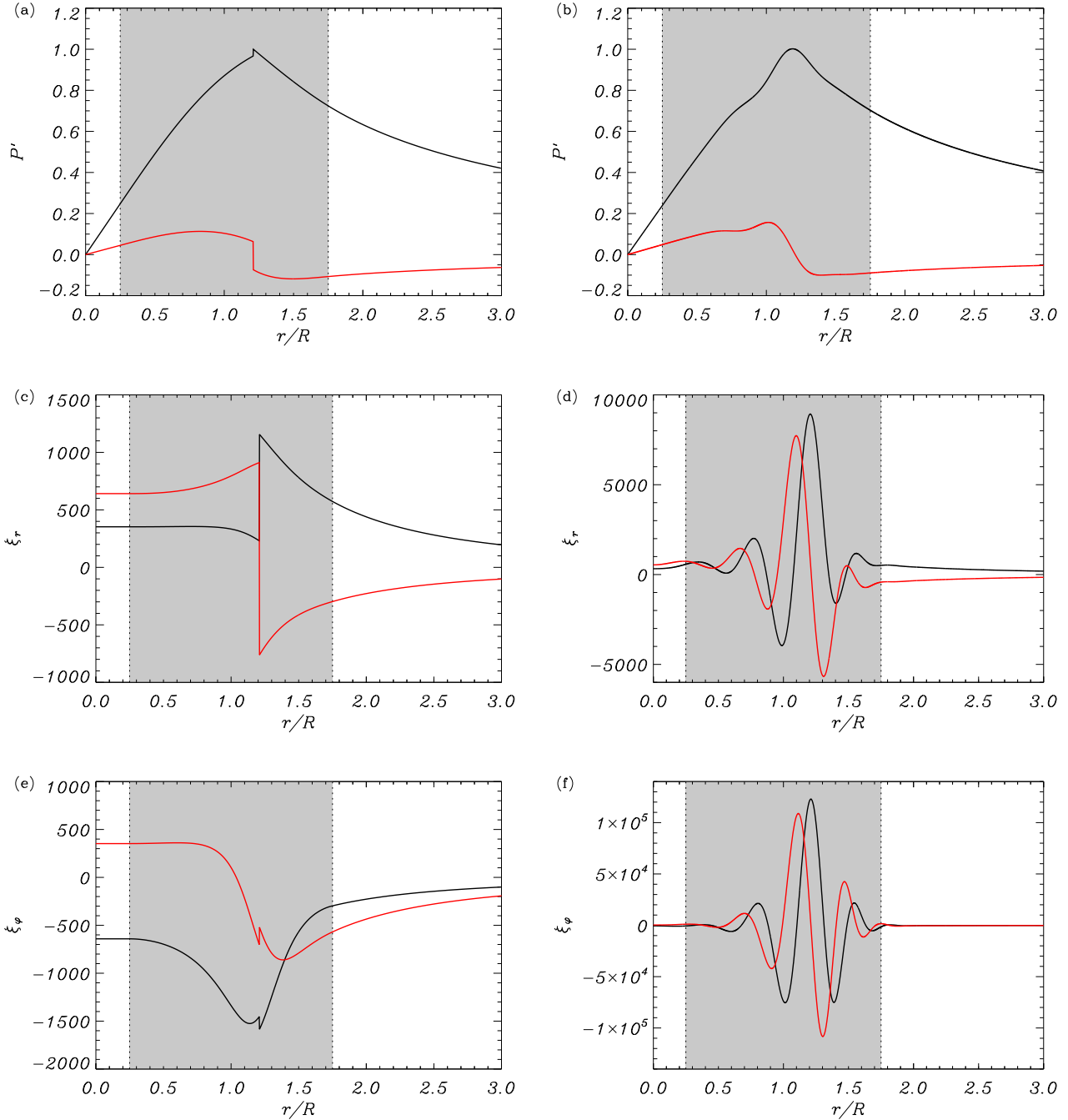


Figure 3. Same as Figure 2 but for $l/R = 1.5$.

width of the oscillatory domain does not decrease below a certain thickness, which is approximately given by Equation (65). Once this minimal thickness is reached, the effect of decreasing η is to produce more and more oscillations in the resonant layer. This phenomenon can be seen in Figure 2.3 of Andries (2003). We observe the same behavior here. The characteristic oscillatory behavior of the resistive eigenfunctions does not disappear for vanishing resistivity so that the ideal eigenfunctions are not recovered. This is a fundamental difference between ideal and resistive eigenmodes.

The resistive results shown here can also be related to the study by Van Doorselaere & Poedts (2007) in a nonuniform

Cartesian slab. They found that, when the nonuniform region spreads over a substantial part of the slab, the global transverse mode loses its global character and gradually becomes indistinguishable from an ordinary resistive mode of the Alfvén spectrum. For a similar experiment in cylindrical geometry see Arregui et al. (2005). Here, we obtain an equivalent result for the resistive kink mode. In the ideal case, however, the kink mode never loses its character as a global mode of the flux tube regardless of the thickness of the nonuniform layer.

Another important result observed in Figures 2 and 3 is the absence of true singularities in the ideal eigenfunctions.

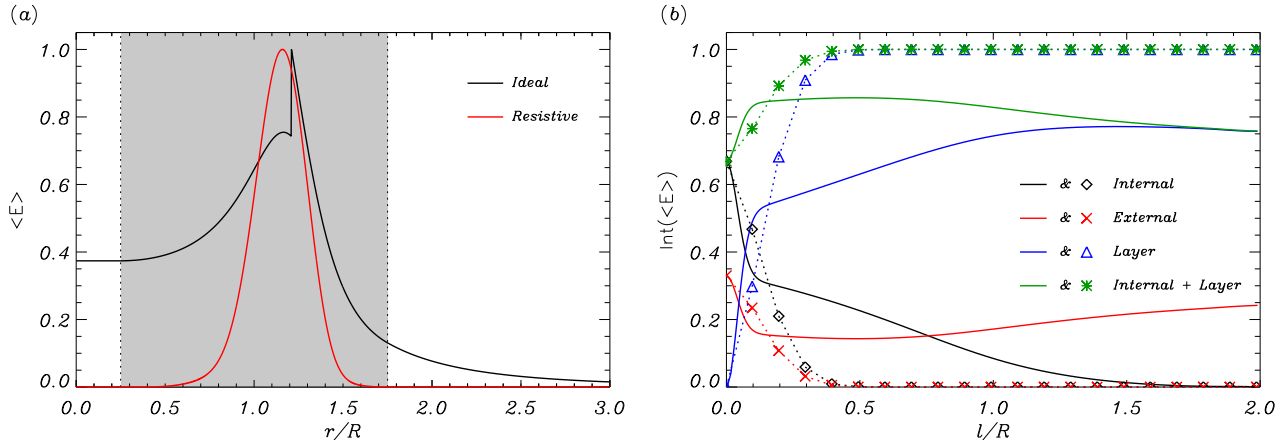


Figure 4. (a) Spatial distribution of the kink mode energy density in a tube with $l/R = 1.5$. The ideal (black) and resistive (red) results are plotted for comparison. The shaded area denotes the nonuniform layer. The plot is normalized so that $\max\langle E \rangle = 1$. (b) Integrated energy in the various regions of the equilibrium flux tube as function of l/R . Solid lines correspond to the ideal results and symbols correspond to the resistive results. The meaning of the various colors is indicated within the Figure. The plot is normalized with respect to the total integrated energy. In all cases we use a sinusoidal variation of density, $\rho_i/\rho_e = 5$, and $L/R = 100$.

Instead, the eigenfunctions have finite jumps at the resonance position (see also Stenuit et al. 1998). As explained in Section 4.2, the finite jumps of the ideal eigenfunctions in the nonuniform layer are caused by the logarithmic term in the Frobenius series. The physical reason for the existence of these jumps is that there is a net flux of energy toward the nonuniform layer so that $\langle S_r \rangle$ (Equation (60)) jumps at the resonance position (see plots of the energy flux in, e.g., Stenuit et al. 1999; Arregui et al. 2011; Goossens et al. 2013). For thin layers, the jump of $\langle S_r \rangle$ is given in Equation (61). The efficiency of energy transfer towards the resonance is determined by the jump of $\langle S_r \rangle$. In the presence of resistivity, the expression of $\langle S_r \rangle$ has additional terms proportional to η , which are of minor importance compared to the ideal term and do not alter the jump of the energy flux (see Arregui et al. 2011). Mathematically, the absence of true singularities is a direct consequence of the fact that wave frequency, ω , is complex. In turn, the singularity condition $\omega^2 = k_z^2 v_A^2(r_A)$ requires r_A to be a complex quantity too. Hence, there is no true singularity at $r = r_A$ because the radial coordinate, r , is obviously real. Instead, there is a finite logarithmic jump of the perturbations at $r = \text{Re}(r_A)$. The jump is finite as long as $\omega_I \neq 0$ so that $\text{Im}(r_A) \neq 0$. When $l/R \ll 1$, $\omega_I^2 \ll \omega_R^2$ and $\text{Im}(r_A) \ll \text{Re}(r_A)$, hence the behavior of the eigenfunctions is quasi-singular in thin layers (Figure 2), although we stress that there is no true singularity even in this case. Conversely, for thick layers ω_I^2 and ω_R^2 are of the same order and there is no hint of singularity in the eigenfunctions (Figure 3). The absence of singularities in the eigenfunctions is a result also found in time-dependent simulations, where the wave perturbations remain finite around the resonance position (see, e.g., Terradas et al. 2006a; Soler et al. 2011b; Pascoe et al. 2013).

5.3. Energy distribution

The distinct form of ideal and resistive eigenfunctions has important repercussions for the computation of the wave energy distribution. The time-averaged total energy density, $\langle E \rangle$, is (e.g., Walker 2005)

$$\langle E \rangle = \frac{1}{2} \left(\rho \mathbf{v} \cdot \mathbf{v}^* + \frac{1}{\mu} \mathbf{b} \cdot \mathbf{b}^* \right), \quad (66)$$

where $\mathbf{v} = -i\omega\xi$ is the velocity perturbation. We use the eigenfunctions for $l/R = 1.5$ displayed in Figure 3 to compute the spatial distribution of $\langle E \rangle$. This is shown in Figure 4(a). As expected, the ideal and resistive results differ. In the resistive case, the energy is essentially confined near the vicinity of the resonance, whereas the amount of energy in the rest of the equilibrium is negligible. The energy spatial distribution depends upon η , so that the smaller η , the more confined is the energy around the resonance position. Conversely, in the ideal case energy spreads over the whole nonuniform layer, and the amount of energy in the internal and external regions is not negligible.

We study how the energy is distributed in the flux tube when l/R varies from $l/R = 0$ to $l/R = 2$ by computing the integrated energy density,

$$\text{Int}(\langle E \rangle) = \int_0^\infty \langle E \rangle r dr. \quad (67)$$

Figure 4(b) displays the integrated energy density in the various regions of the equilibrium as function of l/R . Both ideal and resistive results agree when $l/R = 0$. Around 65% of the wave energy is in the internal plasma and around 35% in the external plasma. The differences between ideal and resistive results arise when l/R increases. In the case of the resistive results, all the energy goes to the nonuniform layer when $l/R \gtrsim 0.5$. Almost no energy is left in the internal and external regions in the resistive case. In the ideal case, most of the energy is in the nonuniform layer too, but the amount of energy in the internal and external plasmas is not negligible even when the transitional layer is very thick. For a fully nonuniform tube, i.e., $l/R = 2$, around 25% of the energy remains located in the external medium in the ideal case.

Recently, Goossens et al. (2013) discussed the energy distribution of kink waves in nonuniform flux tubes. Since they used results from resistive eigenvalues, their conclusion was that almost all the energy is concentrated in the nonuniform layer. Based on this result, they proposed a simple formula to compute the total energy carried by kink waves in the solar atmospheric flux tubes (Goossens et al. 2013, Equation (48)). In view of the results shown here, the conclusions of Goossens et al. (2013) should be reconsidered for the case of the energy distribution of ideal kink waves.

6. ROLE OF THE DENSITY PROFILE

In the previous Section 5, we used a sinusoidal variation of density in the transitional layer. Here, we determine the impact of using other density profiles. In addition to the sinusoidal variation (Equation (63)) we consider a linear profile,

$$\rho_{\text{tr}}(r) = \rho_i - \frac{\rho_i - \rho_e}{l} \left(r - R + \frac{l}{2} \right), \quad (68)$$

and a parabolic profile,

$$\rho_{\text{tr}}(r) = \rho_i - \frac{\rho_i - \rho_e}{l^2} \left(r - R + \frac{l}{2} \right)^2. \quad (69)$$

We have chosen these two profiles for the following reason. The numerical factor F is the only effect of the specific density variation that remains in the TTTB formula for the damping rate (Equation (48)). This is based on the assumption that $r_A \approx R$, so that the formula to compute the factor F is

$$F = \frac{4}{\pi^2} \frac{l}{\rho_i - \rho_e} \left| \frac{d\rho}{dr} \right|_R. \quad (70)$$

Hence, $F = 2/\pi$ for the sinusoidal profile and $F = 4/\pi^2$ for both linear and parabolic profiles. Using these values of F in Equation (48), the same damping rate is predicted for both linear and parabolic profiles. On the other hand, the form of the density profile has no impact at all on the real part of the frequency according to Equation (43). Our first aim here is to check the validity of these predictions.

We must point out that, almost certainly, the true shape of the transitional layer in coronal flux tubes is not any of the three profiles selected here. The second aim of this Section is to determine whether our ignorance about this shape is relevant or, on the contrary, it is unimportant for the behavior of the kink mode.

6.1. Effect on the frequency and damping rate

Figure 5 shows the real and imaginary parts of the fundamental kink mode frequency versus l/R for the three considered density profiles with $l/R = 100$ and $\rho_i/\rho_e = 5$. At first sight, we notice striking differences between the various curves.

We start by analyzing the behavior of ω_R (Figure 5(a)). We find that the density profile affects the value of ω_R beyond the thin layer limit. We compare the results of the three profiles.

1. The result for the sinusoidal profile is the solution that deviates the least from the TT approximation. It deviates from $\omega_R \approx \omega_k$ around $l/R \approx 0.7$, which is a relatively thick layer. The actual ω_R is 18% larger than ω_k when $l/R \approx 2$.
2. The value of ω_R for the linear profile deviates from ω_k around $l/R \approx 0.4$, which is a thinner layer than for the sinusoidal profile. Later, it is the solution that departs the most from the TT approximation. In this case, the actual ω_R is 35% larger than ω_k when $l/R \approx 2$.
3. The solution for the parabolic profile deviates immediately from the TT approximation when l/R increases from zero, although ω_R does not increase as much as for the linear profile. When $l/R \approx 2$, the actual ω_R is 19% larger than ω_k .

We turn to the damping rate (Figure 5(b)). Again, the results for the three profiles are significantly different. Two relevant findings should be stressed.

1. For small l/R the damping rate for the parabolic profile is closer to the solution for the sinusoidal profile than to that for the linear profile, although the TTTB formula predicts the same damping rate for both linear and parabolic profiles. The reason for this discrepancy is that $r_A \approx R$ is a bad approximation for the parabolic profile. For the parabolic dependence, the density is not symmetric with respect to $r = R$ and the actual resonance position is not located at the center of the transitional layer. Consequently, using $F = 4/\pi^2$ for the parabolic profile causes the TTTB formula to overestimate the actual damping rate. Accidentally, using $F = 2/\pi$ as for sinusoidal profile provides an approximate damping rate closer to the actual value.
2. The damping rate for the linear profile is nonmonotonic. For the parameters used in Figure 5, there is a turning point at $l/R \approx 0.9$. As a consequence, we find that the behavior for $l/R \gtrsim 0.9$ is the opposite one to the prediction of the TTTB formula, i.e., the thicker the layer, the weaker the damping. In addition, an intersection of the actual damping rate with the TTTB approximate value occurs for thick layers regardless the density contrast. The presence of the turning point has also the consequence that two different values of l/R produce the same damping rate.

The results for the linear density profile shown here can be compared with the study by Tatsuno & Wakatani (1998). These authors investigated the resonant damping of surface Alfvén waves in a Cartesian slab in the limit of propagation nearly perpendicular to the magnetic field. They took a linear variation of density in a nonuniform layer surrounding the slab dense core. Although the Cartesian model used by Tatsuno & Wakatani (1998) is different from the cylindrical waveguide used here, the present results for the behavior of the kink mode frequency and damping rate are similar to those found by Tatsuno & Wakatani (1998), as can be seen by comparing their Figure 2 with our Figure 5.

An explanation for the different behavior of the damping rate for the three profiles can be found in the dependence of the jump of the radial component of the energy flux with l/R . We compute the radial energy flux at the resonance, F_r , as (see, e.g., Wright & Thompson 1994; Arregui et al. 2011)

$$F_r = r_A \left| [\langle S_r \rangle]_{r_A} \right|, \quad (71)$$

where $[\langle S_r \rangle]_{r_A}$ denotes the jump of $\langle S_r \rangle$ at the resonance. Following Wright & Thompson (1994), see also Arregui et al. (2011), an alternative way to obtain the kink mode damping rate (in absolute value) is computing the ratio of F_r to the total integrated energy, $\text{Int}(\langle E \rangle)$, namely

$$|\omega_I| = \frac{F_r}{\text{Int}(\langle E \rangle)}. \quad (72)$$

This result is displayed in Figure 6(a), where it is compared to the actual ω_I plotted in Figure 5(b). An excellent agreement between both results is obtained. The form of the density profile affects the evolution F_r when l/R increases. In the case of the linear profile, we find that for thick layers F_r gets smaller when l/R increases. As a consequence, the efficiency of resonant damping becomes lower when the thickness of the layer

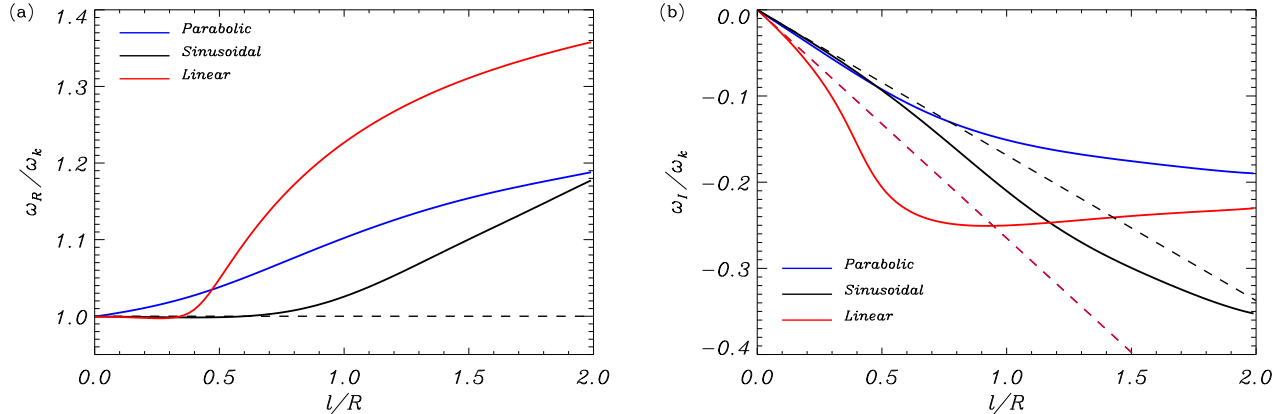


Figure 5. (a) Real part and (b) imaginary part of the kink mode frequency versus l/R . The line color denotes the density profile considered in the nonuniform layer (indicated within the figures). The dashed lines are the TTTB analytic results (Equations (43) and (48)). The red dashed line applies to both linear and parabolic profiles. In all cases we use $\rho_i/\rho_e = 5$ and $L/R = 100$.

grows. Conversely, for the parabolic and sinusoidal profiles F_r gets larger when l/R increases.

In summary, we find that beyond the limiting case of thin nonuniform layers, the specific form of the density profile strongly influences the kink mode frequency and damping rate. Among the three profiles used here, the sinusoidal variation is the profile for which the extrapolation of the TTTB approximation works the best. For other density profiles different from the sinusoidal one, the error done by the TTTB approximation when used beyond its range of applicability can be much larger depending on the model parameters. A detailed study of the error done due to the TTTB approximation will be presented in the forthcoming second part of this work.

6.2. Effect on the energy distribution

Finally, we determine the effect of the transverse density profile on the wave energy distribution. To this end, we compute $\text{Int}(\langle E \rangle)$ in the various regions of the equilibrium as function of l/R . We use the ideal eigenfunctions obtained with the Frobenius method. Figure 6(b) shows the ratio of the integrated energy inside the flux tube, i.e., the integrated energy in the internal homogeneous medium plus the integrated energy in the nonuniform layer, to the integrated energy in the external plasma. This ratio informs us about the amount of energy confined within the flux tube compared to the amount of energy located in the external medium. When $l/R = 0$, the energy inside the flux tube is about twice the energy in the external medium. Again, we find important differences between the results obtained with the three density profiles when l/R increases.

Among the three profiles, the sinusoidal one is the profile for which the confinement of energy inside the flux tube is largest, while the linear profile is the profile that produces the poorest confinement of energy. When $l/R = 2$, the amount of energy inside the tube is about 3 times larger than outside for the sinusoidal profile, whereas for the linear profile the energy inside the tube is only 1.5 times larger than the external energy, approximately. The result for the parabolic profile is in between those of the linear and sinusoidal profiles.

As for the frequency and damping rate, the results here show a strong dependence of the energy distribution on the specific density variation in the nonuniform layer. For com-

parison, we have repeated the computations of Figure 6(b) but using the resistive eigenfunctions (not shown here). In the resistive case, there are no differences between the various profiles because all the energy quickly goes to the dissipative layer when l/R increases from zero, so that the amount of energy in the external plasma becomes negligible regardless of the density profile (see Figure 4(b)).

7. DISCUSSION

In this article, we developed an analytic technique to compute the dispersion relation and the eigenfunctions of transverse MHD waves in pressureless cylindrical flux tubes with nonuniform transitional layers of arbitrary thickness. The method allows to consider an arbitrary spatial variation of density in the nonuniform layer. Unlike previous works that considered thick transitional layers (see, e.g., Van Doorselaere et al. 2004; Arregui et al. 2005), the technique does not rely on the use of resistive MHD computations. We consider the linearized ideal MHD equations and use the Method of Frobenius to express the solution for the total pressure perturbation in the nonuniform layer as a combination of a singular and a regular series around the Alfvén resonance position (see, e.g., Zhu & Kivelson 1988; Hollweg 1990b,a; Wright & Thompson 1994; Cally & Andries 2010). Specific results for kink modes were produced as an application of the technique. We compared the ideal results obtained with the Frobenius method with the fully numerical solution of the resistive eigenvalue problem in the limit of small resistivity.

We find that the frequency and resonant damping rate of kink waves is the same in both ideal and resistive cases. The comparison of the results obtained with different density profiles in the nonuniform layer revealed that the specific form of the density variation affects both the frequency and the damping rate beyond the limit of thin layers. In particular, the accuracy of the TTTB approximation for the ratio of the damping time to the period is very sensitive to the density profile. The previous papers that studied the effect of thick layers (Van Doorselaere et al. 2004; Arregui et al. 2005) restricted themselves to a sinusoidal variation and did not consider other density profiles. The error done with the TTTB formula of τ_D/P might be larger than 25%, which was estimated by Van Doorselaere et al. (2004) for the specific case of a sinusoidal variation. This will be explored in detail in the

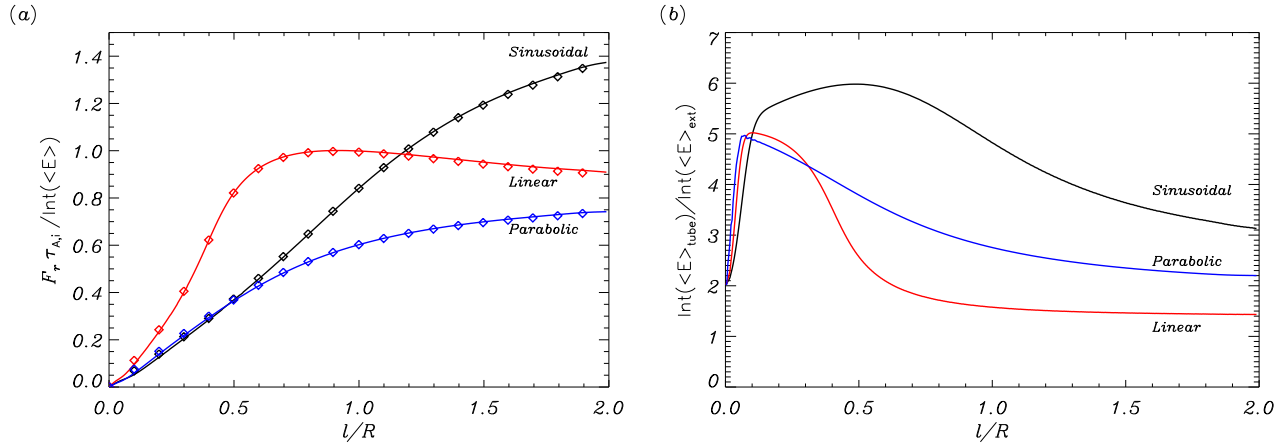


Figure 6. (a) Damping rate as function of l/R . Solid lines are the ratio of the radial energy flux at the resonance, F_r , to the integrated total energy. Symbols are the absolute value of ω_1 plotted in Figure 5(b). In both cases, the damping rate is given in units of the internal Alfvén travel time, $\tau_{A,i} = L/v_{A,i}$. (b) Ratio of the integrated energy inside the flux tube (internal medium + nonuniform layer) to the integrated energy in the external plasma as function of l/R . In both panels, the line color denotes the density profile considered in the nonuniform layer. In all cases we use $\rho_i/\rho_e = 5$ and $L/R = 100$.

second part of this investigation.

The ideal MHD eigenfunctions are slightly different for thin nonuniform layers but strongly different for thick layers from their resistive MHD counterparts. The ideal eigenfunctions show finite jumps at the Alfvén resonance position as a consequence of the net energy inflow into the resonance from both sides. In the resistive case, the jumps are replaced by spatial oscillations of large amplitude, which are very localized around the resonance position, so that the kink mode loses its global character and becomes indistinguishable from a resistive Alfvén mode (Van Doorselaere & Poedts 2007). This raises a fundamental theoretical problem about the correspondence of ideal MHD solutions and resistive MHD solutions (see, e.g., Poedts & Kerner 1991; Ruderman et al. 1995; Andries 2003).

Importantly, we stress the absence of singularities in the eigenfunctions. From the mathematical point of view, the absence of singularities is a direct consequence of the fact that that normal mode frequency, ω , is complex. Equivalently, singularities are also absent in the case of propagating waves, because k_z is then complex. When either ω or k_z are complex, the resonance condition $\omega^2 = k_z^2 v_A^2(r_A)$ implies that the resonance position, r_A , is in the complex plane. For a singularity to be present, r_A has to be on the real axis. This would be the case, for example, of a line-tied flux tube that is externally forced to oscillate at a certain frequency, so that both ω and k_z are fixed real quantities and, therefore, r_A is real. For damped normal modes, however, singularities do not occur, although we can call the position $r = \text{Re}(r_A)$ a quasi-singularity.

The different form of the eigenfunctions affects the spatial distribution of energy carried by the waves. In the resistive case, the wave energy distribution is essentially confined in the vicinity of the resonance position regardless of the transverse density profile. In the ideal case, the energy spreads over the whole flux tube, and the amount of energy that is confined within the waveguide or is located in the external medium depends on the transverse density profile.

The question of what description, i.e., ideal or resistive, is the best representation for the observed waves in the solar atmosphere is open for discussion. This question is not only of obvious theoretical importance but also of practical importance for the interpretation of the energy content and distribution in kink waves (Goossens et al. 2013). In the solar at-

mosphere magnetic resistivity is very small but it is definitely nonzero. The problem of how to reconcile the observed transverse global oscillations with the resistive eigenmodes is a serious challenge for future theoretical studies.

Another important issue is how to relate the results from normal modes with those of the time-dependent solution. Normal modes provide consistent values of period and damping time when compared with those obtained from the time-dependent solution (e.g., Terradas et al. 2006a). However, time-dependent simulations show that the dynamics in the vicinity of the resonance after several periods does not correspond to the behavior expected from the normal mode. As the global oscillation damps, the energy fed into the inhomogeneous layer is used to generate small-scale motions near the resonance position. The amplitude of these small-scale motions first grows in time due to the energy transfer from the global mode. Later, they are damped in the presence of resistivity, while they remain undamped in the ideal case (see Figure 6 of Terradas et al. 2006a). Thus, normal modes satisfactorily provide a description of the flux tube global oscillation but do not fully capture the small-scale dynamics in the inhomogeneous layer. The degree to which normal mode eigenfunctions remain a good approximation to the actual plasma motions as time increases is a very relevant question. Previous papers by, e.g., Cally (1991) and Cally & Maddison (1997) may be a useful guide to establish the link between the modal analysis of oscillations and the actual time-dependent evolution in inhomogeneous plasmas.

Here, we focused on studying the effect of transverse density variation, while density stratification along the flux tube was neglected. The effect of longitudinal stratification on standing waves was determined by Andries et al. (2005) and Dymova & Ruderman (2006) in the TB approximation and by Arregui et al. (2005) for fully nonuniform tubes. These authors found that the kink mode period and damping time are weakly dependent on longitudinal stratification, while the ratio of the damping time to the period is completely independent of stratification. The effect of longitudinal stratification on propagating waves was studied by Soler et al. (2011b), who found that longitudinal stratification can either amplify or attenuate the wave, depending on whether the density decreases or increases toward the direction of wave propagation, respectively. Thus, the amplitude variation of propa-

gating kink waves along stratified tubes is determined by the combined effect of resonant absorption and density stratification. Other effects as, e.g., the presence of mass flows (e.g., Terradas et al. 2010a; Soler et al. 2011a) and magnetic twist (e.g., Terradas & Goossens 2012) can also have some influence on the kink wave damping rate.

Finally, the results of this article suggest that our ignorance about the true density profile in the nonuniform layer might be very relevant for seismology of solar flux tubes as, e.g., coronal loops, using the observed period and damping rate of transverse oscillations in combination with inversion schemes based on the TTTB approximation (Goossens et al. 2008, 2012b). These schemes are often used beyond the theoretical range of applicability of the TTTB approximation and ignore the influence of the specific density profile. Unfortunately, present-day observations do not have enough spatial resolution to determine the shape of the transitional layer, and seismological inversion schemes usually adopt an ad hoc density variation. As shown here, deviations from the TTTB approximation can be large even for relatively thin nonuniform layers depending on the density profile used. As a consequence, the error done by the inversion schemes and the reliability of the inferred parameters are uncertain. The impact of the transverse density profile on seismically inferred parameters will be explored in the forthcoming continuation of this article.

We thank J. L. Ballester and I. Arregui for reading a draft of this paper and for giving useful comments. The authors acknowledge support from MINECO and FEDER funds through project AYA2011-22846, and from CAIB through the ‘Grups Competitius’ program and FEDER funds. M.G. acknowledges support from KU Leuven via GOA/2009-009. The research of M.G. has partially been funded by the Interuniversity Attraction Poles Programme initiated by the Belgian Science Policy Office (IAP P7/08 CHARM). J.T. acknowledges support from MINECO through a Ramón y Cajal grant.

REFERENCES

- Andries, J. 2003, PhD thesis, KU Leuven
 Andries, J., Goossens, M., Hollweg, J. V., Arregui, I., & Van Doorselaere, T. 2005, *A&A*, 430, 1109
 Andries, J., Tirry, W. J., & Goossens, M. 2000, *ApJ*, 531, 561
 Arregui, I., Andries, J., Van Doorselaere, T., Goossens, M., & Poedts, S. 2007, *A&A*, 463, 333
 Arregui, I., Soler, R., Ballester, J. L., & Wright, A. N. 2011, *A&A*, 533, A60
 Arregui, I., Terradas, J., Oliver, R., & Ballester, J. L. 2008, *ApJ*, 682, L141
 Arregui, I., Van Doorselaere, T., Andries, J., Goossens, M., & Kimpe, D. 2005, *A&A*, 441, 361
 Aschwanden, M. J., de Pontieu, B., Schrijver, C. J., & Title, A. M. 2002, *Sol. Phys.*, 206, 99
 Aschwanden, M. J., Fletcher, L., Schrijver, C. J., & Alexander, D. 1999, *ApJ*, 520, 880
 Aschwanden, M. J., Nightingale, R. W., Andries, J., Goossens, M., & Van Doorselaere, T. 2003, *ApJ*, 598, 1375
 Bray, R. J., & Loughhead, R. E. 1974, *The solar chromosphere*
 Cally, P. S. 1986, *Sol. Phys.*, 103, 277
 —. 1991, *Journal of Plasma Physics*, 45, 453
 —. 2003, *Sol. Phys.*, 217, 95
 Cally, P. S., & Andries, J. 2010, *Sol. Phys.*, 266, 17
 Cally, P. S., & Maddison, S. T. 1997, *Journal of Plasma Physics*, 57, 591
 De Pontieu, B., McIntosh, S. W., Carlsson, M., et al. 2007, *Science*, 318, 1574
 Dymova, M. V., & Ruderman, M. S. 2006, *A&A*, 457, 1059
 Edwin, P. M., & Roberts, B. 1983, *Sol. Phys.*, 88, 179
 Goedbloed, J. P. 1983, *Lecture notes on ideal magnetohydrodynamics*, Tech. Rep. 83–145, Rijnhuizen Report
 Goedbloed, J. P., & Poedts, S. 2004, *Principles of magnetohydrodynamics* (Cambridge University Press)
 Goossens, M., Andries, J., & Aschwanden, M. J. 2002, *A&A*, 394, L39
 Goossens, M., Andries, J., Soler, R., et al. 2012a, *ApJ*, 753, 111
 Goossens, M., Arregui, I., Ballester, J. L., & Wang, T. J. 2008, *A&A*, 484, 851
 Goossens, M., Hollweg, J. V., & Sakurai, T. 1992, *Sol. Phys.*, 138, 233
 Goossens, M., Ruderman, M. S., & Hollweg, J. V. 1995, *Sol. Phys.*, 157, 75
 Goossens, M., Soler, R., Arregui, I., & Terradas, J. 2012b, *ApJ*, 760, 98
 Goossens, M., Terradas, J., Andries, J., Arregui, I., & Ballester, J. L. 2009, *A&A*, 503, 213
 Goossens, M., Van Doorselaere, T., Soler, R., & Verth, G. 2013, *ApJ*, 768, 191
 Hollweg, J. V. 1990a, *Planet. Space Sci.*, 38, 1017
 —. 1990b, *J. Geophys. Res.*, 95, 2319
 Hollweg, J. V., & Yang, G. 1988, *J. Geophys. Res.*, 93, 5423
 Hood, A. W., Ruderman, M., Pascoe, D. J., et al. 2013, *A&A*, 551, A39
 Ionson, J. A. 1978, *ApJ*, 226, 650
 Lee, M. A., & Roberts, B. 1986, *ApJ*, 301, 430
 Nakariakov, V. M., Ofman, L., Deluca, E. E., Roberts, B., & Davila, J. M. 1999, *Science*, 285, 862
 Pascoe, D. J., Hood, A. W., de Moortel, I., & Wright, A. N. 2012, *A&A*, 539, A37
 Pascoe, D. J., Hood, A. W., De Moortel, I., & Wright, A. N. 2013, *A&A*, 551, A40
 Pascoe, D. J., Wright, A. N., & De Moortel, I. 2010, *ApJ*, 711, 990
 Poedts, S., & Kerner, W. 1991, *Physical Review Letters*, 66, 2871
 Ruderman, M. S., & Roberts, B. 2002, *ApJ*, 577, 475
 Ruderman, M. S., & Terradas, J. 2013, *A&A*, in press
 Ruderman, M. S., Tirry, W., & Goossens, M. 1995, *Journal of Plasma Physics*, 54, 129
 Sakurai, T., Goossens, M., & Hollweg, J. V. 1991, *Sol. Phys.*, 133, 227
 Sedláček, Z. 1971, *Journal of Plasma Physics*, 5, 239
 Sewell, G. 2005, *The Numerical Solution of Ordinary and Partial Differential Equations* (Wiley & Sons)
 Soler, R., Oliver, R., & Ballester, J. L. 2009a, *ApJ*, 707, 662
 Soler, R., Oliver, R., Ballester, J. L., & Goossens, M. 2009b, *ApJ*, 695, L166
 Soler, R., Terradas, J., & Goossens, M. 2011a, *ApJ*, 734, 80
 Soler, R., Terradas, J., Verth, G., & Goossens, M. 2011b, *ApJ*, 736, 10
 Stenuit, H., Keppens, R., & Goossens, M. 1998, *A&A*, 331, 392
 Stenuit, H., Tirry, W. J., Keppens, R., & Goossens, M. 1999, *A&A*, 342, 863
 Tataronis, J., & Grossmann, W. 1973, *Zeitschrift für Physik*, 261, 203
 Tatsuno, T., & Wakatani, M. 1998, *Journal of the Physical Society of Japan*, 67, 2322
 Terradas, J., & Goossens, M. 2012, *A&A*, 548, A112
 Terradas, J., Goossens, M., & Ballai, I. 2010a, *A&A*, 515, A46
 Terradas, J., Goossens, M., & Verth, G. 2010b, *A&A*, 524, A23
 Terradas, J., Oliver, R., & Ballester, J. L. 2006a, *ApJ*, 642, 533
 —. 2006b, *Royal Society of London Philosophical Transactions Series A*, 364, 547
 Tomczyk, S., McIntosh, S. W., Keil, S. L., et al. 2007, *Science*, 317, 1192
 Van Doorselaere, T., Andries, J., Poedts, S., & Goossens, M. 2004, *ApJ*, 606, 1223
 Van Doorselaere, T., & Poedts, S. 2007, *Plasma Physics and Controlled Fusion*, 49, 261
 Walker, A. D. M. 2005, *Magnetohydrodynamic Waves in Geospace*, Series in Plasma Physics, (Institute of Physics Publishing)
 Wright, A. N., & Thompson, M. J. 1994, *Physics of Plasmas*, 1, 691
 Zhu, X., & Kivelson, M. G. 1988, *J. Geophys. Res.*, 93, 8602

APPENDIX

EXPRESSIONS OF COEFFICIENTS

The expressions of the coefficients a_k and s_k are as follows,

$$a_0 = 1, \tag{A1}$$

$$a_1 = -\frac{2\rho_1 - 2\rho_2 r_A}{3\rho_1 r_A} a_0, \tag{A2}$$

$$a_2 = -\frac{9\rho_1 r_A a_1 + (2\rho_1 - 2\rho_2 r_A - 4\rho_3 r_A^2 - m^2 \rho_1) a_0}{8\rho_1 r_A^2}, \tag{A3}$$

$$a_3 = -\frac{1}{15\rho_1 r_A^2} \left[(4\rho_2 r_A^2 + 20\rho_1 r_A) a_2 + (-3\rho_3 r_A^2 + 3\rho_2 r_A + 6\rho_1 - m^2 \rho_1) a_1 \right. \\ \left. + \left(-6\rho_4 r_A^2 - 6\rho_3 r_A + \frac{\omega^2 r_A^2}{B^2/\mu} \rho_1^2 - m^2 \rho_2 \right) a_0 \right], \quad (\text{A4})$$

$$a_4 = -\frac{1}{24\rho_1 r_A^2} \left[\sum_{j=0}^3 (j+2)(2j-4) r_A^2 \rho_{5-j} a_j + \sum_{j=0}^3 (j+2)(4j-5) r_A \rho_{4-j} a_j \right. \\ \left. + \sum_{j=0}^2 \left((j+2)(2j-1) - m^2 \right) \rho_{3-j} a_j + \sum_{j=0}^1 \sum_{l=0}^{1-j} \frac{\omega^2 r_A^2}{B^2/\mu} \rho_{l+1} \rho_{2-j-l} a_j + 2 \frac{\omega^2 r_A}{B^2/\mu} \rho_1^2 a_0 \right], \quad (\text{A5})$$

$$a_k = -\frac{1}{k(k+2)\rho_1 r_A^2} \left[\sum_{j=0}^{k-1} (j+2)(2j-k) r_A^2 \rho_{k-j+1} a_j + \sum_{j=0}^{k-1} (j+2)(4j-2k+3) r_A \rho_{k-j} a_j \right. \\ \left. + \sum_{j=0}^{k-2} \left((j+2)(2j-k+3) - m^2 \right) \rho_{k-j-1} a_j + \sum_{j=0}^{k-3} \sum_{l=0}^{k-j-3} \frac{\omega^2 r_A^2}{B^2/\mu} \rho_{l+1} \rho_{k-j-l-2} a_j \right. \\ \left. + \sum_{j=0}^{k-4} \sum_{l=0}^{k-j-4} 2 \frac{\omega^2 r_A}{B^2/\mu} \rho_{l+1} \rho_{k-j-l-3} a_j + \sum_{j=0}^{k-5} \sum_{l=0}^{k-j-5} \frac{\omega^2}{B^2/\mu} \rho_{l+1} \rho_{k-j-l-4} a_j \right], \quad \text{for } k \geq 5, \quad (\text{A6})$$

$$s_0 = 1, \quad (\text{A7})$$

$$s_1 = 0, \quad (\text{A8})$$

$$s_2 = 0, \quad (\text{A9})$$

$$s_3 = \frac{1}{3\rho_1 r_A^2} \left[\left(m^2 \rho_2 - \frac{\omega^2 r_A^2}{B^2/\mu} \rho_1^2 \right) s_0 - C \left(4r_A^2 \rho_1 a_1 + (r_A^2 \rho_2 + 5r_A \rho_1) a_0 \right) \right], \quad (\text{A10})$$

$$s_4 = -\frac{1}{8\rho_1 r_A^2} \left[9\rho_1 r_A s_3 + \left(2 \frac{\omega^2 r_A}{B^2/\mu} \rho_1^2 + 2 \frac{\omega^2 r_A^2}{B^2/\mu} \rho_1 \rho_2 - m^2 \rho_3 \right) s_0 \right. \\ \left. + C \left(6r_A^2 \rho_1 a_2 + 3r_A^2 \rho_2 a_1 + 9r_A \rho_1 a_1 + 3(r_A \rho_2 + \rho_1) a_0 \right) \right], \quad (\text{A11})$$

$$s_k = -\frac{1}{k(k-2)\rho_1 r_A^2} \left\{ \sum_{j=0}^{k-1} j(2j-k-2) r_A^2 \rho_{k-j+1} s_j + \sum_{j=0}^{k-1} j(4j-2k-1) r_A \rho_{k-j} s_j \right. \\ \left. + \sum_{j=0}^{k-2} \left[\left(j(2j-k+1) - m^2 \right) \rho_{k-j-1} s_j + C(3j-k+4) r_A^2 \rho_{k-j-1} a_j \right] \right. \\ \left. + \sum_{j=0}^{k-3} \left[\sum_{l=0}^{k-j-3} \frac{\omega^2 r_A^2}{B^2/\mu} \rho_{l+1} \rho_{k-j-l-2} s_j + C(6j-2k+11) r_A \rho_{k-j-2} a_j \right] \right. \\ \left. + \sum_{j=0}^{k-4} \left[\sum_{l=0}^{k-j-4} 2 \frac{\omega^2 r_A}{B^2/\mu} \rho_{l+1} \rho_{k-j-l-3} s_j + C(3j-k+7) \rho_{k-j-3} a_j \right] \right. \\ \left. + \sum_{j=0}^{k-5} \sum_{l=0}^{k-j-5} \frac{\omega^2}{B^2/\mu} \rho_{l+1} \rho_{k-j-l-4} s_j \right\}, \quad \text{for } k \geq 5. \quad (\text{A12})$$